Journal of Industrial and Engineering Chemistry 25 (2015) 338–343

Contents lists available at ScienceDirect

Journal of Industrial and Engineering Chemistry

journal homepage: www.elsevier.com/locate/jiec

Enhanced activity of Cu–Fe/SiO_2 catalyst for CO hydrogenation to higher alcohols by pretreating the support with ammonia

Ruili Lu, Dongsen Mao *, Jun Yu, Qiangsheng Guo

Research Institute of Applied Catalysis, School of Chemical and Environmental Engineering, Shanghai Institute of Technology, Shanghai 201418, PR China

ARTICLE INFO

Article history:
Received 24 August 2014
Received in revised form 11 November 2014
Accepted 18 November 2014
Available online 25 November 2014

Keywords:
Cu–Fe/SiO_2
Higher alcohols
CO hydrogenation
Ammonia
Silica pretreatment

ABSTRACT

The effect of support pretreatment with ammonia on the performance of Cu–Fe/SiO_2 catalyst for higher alcohols synthesis from syngas was studied by CO hydrogenation, X-ray diffraction, N_2 adsorption–desorption, temperature-programmed reduction of H_2, Fourier transform infrared spectroscopy, N_2O chemisorption and temperature-programmed desorption of adsorbed CO. The results indicated that the pretreatment of SiO_2 with ammonia resulted in the formation of more active sites of Cu and higher dispersion of Fe species on the catalyst surface and enhanced the synergistic effect between the copper and iron species. As a result, the CO conversion and the space time yield of alcohols of the Cu–Fe/SiO_2 catalyst increased from 14.8% and 89.0 g kg^{-1} h^{-1} to 17.4% and 107.0 g kg^{-1} h^{-1}, respectively.

Introduction

As increasing awareness of global warming and petroleum sources crises, looking for a new alternative energy has aroused extensive attention. In the past decades, a novel technology for the production of mixed alcohols from synthesis gas derived from coal, natural gas and biomass has attracted more attention in academic and industrial fields [1]. The heterogeneous catalysts for the mixed alcohols synthesis can be broadly divided into noble metal-based catalysts and non-noble metal-based catalysts. The noble metal-based catalysts which usually include Rh supported on various oxides are mainly used for the conversion of syngas to ethanol and other C_2-oxygenates [2,3]. However, these catalysts have little attraction for commercial application due to high cost of their large scale utilization [4,5]. The major non-noble metal-based catalysts are classified as modified methanol synthesis catalysts, modified Fischer–Tropsch (F–T) synthesis catalysts, and alkali-doped molybdenum catalysts [2,6]. Among these non-noble metal catalysts, the Cu-based catalysts containing metals active toward F–T synthesis (Fe, Co or Ni), such as Cu–Co, are considered as the most promising candidate for mixed alcohols synthesis from syngas [7,8]. Nevertheless, the Cu–Co catalysts generally suffer from poor stability in long-term run and the low selectivity to higher alcohols [9–11].

In recent years, in addition to Cu–Co catalyst, Cu–Fe based catalysts with good performance for higher alcohols synthesis have been reported extensively [9–17]. Although much effort has been devoted to the development of Cu–Fe based catalyst, however, several problems remain not well-resolved, such as low selectivity to alcohols, high hydrocarbons selectivity and products with plenty of water [11]. So, it is necessary to further improve the performance of the Cu–Fe-based catalyst. At present, there are three main methods to improve the performance of Cu–Fe-based catalyst: first is to add suitable additives for modification [9,10,18]; second is to find suitable methods to prepare the catalyst [11,15,16], and the third is the application of appropriate supports [12,14,19]. For instance, Ding et al. [12] recently found that the Cu–Fe catalyst supported on bimodal pore SiO_2 exhibited favorite catalytic activity and high selectivity of $C_{2+}OH$, due to the well dispersion of active metal sites and high diffusion efficiency of products inside the bimodal pore structures.

It is well known that besides the textural properties, the chemical properties of the support surface take a central role in the performance of supported catalysts [20–28]. For example, Jiang et al. [20] reported that pretreatment of the silica with nC_1–C_5 alcohols could improve the CO conversion and selectivity to C_2-oxygenates of Rh–Mn–Li/SiO_2 catalyst, due to the increased dispersion of Rh and ratio of Rh^+/Rh^0 sites. Yu et al. [22] found that the performance of Rh–Mn–Li/SiO_2 catalyst for the synthesis of C_2-oxygenates from syngas was enhanced by calcination of the silica support at a proper temperature, owing to the achieving of an appropriate amount of Si–OH groups which can gain a moderate

* Corresponding author. Tel.: +86 21 6087 3625; fax: +86 21 6087 3625.
E-mail address: dsmao@sit.edu.cn (D. Mao).

http://dx.doi.org/10.1016/j.jiec.2014.11.013
1226-086X/

interaction between Rh and Mn and ultimately increases the selectivity to C_2-oxygenates. Zhang et al. [24] found that the Co/SiO_2 catalysts prepared from pretreated supports with organic solvents such as acetic acid, ethanol, 1-propanol or 1-butanol, exhibited higher catalytic activity due to the higher dispersion and higher reducibility of the supported cobalt. Lv et al. [26] reported that the modified silica support with ethylene glycol decreased the decomposition temperature of impregnated nickel nitrate and enhanced the metal-support interaction, and consequently increased the stability and catalytic activity of Ni/SiO_2 catalyst for dry reforming of CH_4. Shi et al. [27] found that Co catalyst supported on $(CH_3)_3$-modified SiO_2 exhibited higher activity and C_{5+} hydrocarbons selectivity and lower CH_4 selectivity due to yielding a highly hydrophobic silica-like surface by $(CH_3)_3$-group modification of SiO_2. On the other hand, Zhang et al. [28] studied the effect of hydrothermal treatment of alumina in the presence of a medium (ammonia, ammonium nitrate, acetic acid, or ethanol) on the performance of Co/Al_2O_3 catalyst for F–T synthesis and found that Co catalyst supported on ammonia and ammonium nitrate-treated Al_2O_3 showed higher reducibility and more bridged-form CO, and hence exhibited higher activity and C_{5+} hydrocarbons selectivity. Based on the above, we report an effective method to enhance the performance of the Cu–Fe/SiO_2 catalyst for the synthesis of higher alcohols from syngas by the pretreatment of SiO_2 with ammonia in the present work.

Experimental

Catalyst preparation

A commercial silica gel (Qingdao Haiyang Chemicals Company, China) was dried at 110 °C for 4 h, and then used as the support in this study. For support pretreatment, the silica gel (3 g) was placed along with a medium (5 vol.% ammonia) in a Teflon lined autoclave. The system temperature was raised to 200 °C ramping at 10 °C/min and kept at this temperature for 3 h. Then the sample was filtrated and dried overnight at 110 °C. The obtained sample was named as SiO_2–N. For comparison, the same method was used for the support SiO_2 pretreated by H_2O, which was named as SiO_2–H.

The Cu–Fe/SiO_2 catalysts were prepared by co-impregnating the silica supports prepared above with the aqueous solutions containing cupric nitrate and ferric nitrate. The impregnated catalysts were dried at 110 °C for 10 h and calcined in static air at 350 °C for 4 h. Both the Cu and Fe loadings of the catalysts were 10 wt.%. The $Cu(NO_3)_2{\cdot}3H_2O$ and $Fe(NO_3)_3{\cdot}9H_2O$ were of analytical purity and purchased from Chinese Sinopharm Chemical Reagent Co., Ltd., China.

Catalyst testing

CO hydrogenation reaction was carried out in a fixed-bed micro-reactor with length of ~350 mm and internal diameter of ~5 mm [19]. The catalyst (0.3 g) was loaded between quartz wool and axially centered in the reactor tube, with the temperature monitored by a thermocouple close to the catalyst bed. Prior to reaction, the catalyst was heated to 300 °C (heating rate = 3 °C/min) and reduced with a H_2/N_2 mixture (50 mL/min, V_{H2}/V_{N2} = 1:9) for 3 h at atmospheric pressure. The catalyst was then cooled down to 250 °C and the reaction started as gas flow was switched to a H_2/CO mixture (30 mL/min, V_{H2}/V_{CO} = 2:1) at 3 MPa. All post-reactor lines and valves were heated to 150 °C for preventing the possible condensation of products. The products were analyzed for both oxygenates and hydrocarbons on-line by Agilent GC 6820 equipped with a flame ionization detector (FID) and a thermal conductivity detector (TCD). The conversion of CO was calculated based on the fraction of CO that formed carbon-containing products according to: % conversion = $(\sum n_i M_i / M_{CO}) \times 100$, where n_i is the number of carbon atoms in product I; M_i is the percentage of product i detected, and M_{CO} is the percentage of CO in the syngas feed. The selectivity of a certain product was calculated based on carbon efficiency using the formula % $S_i = (n_i C_i / \sum n_i C_i) \times 100$, where n_i and C_i are the carbon number and molar concentration of the ith product, respectively. The carbon balance and mass balance were 100 ± 5%.

Sample characterization

XRD patterns were recorded on a PANalytical X'Pert instrument using Ni filtered Cu Kα radiation (λ = 0.15418 nm) at 40 kV and 40 mA. Two theta angles ranged from 15° to 80° with a scanning rate of 6°/min.

BET surface areas, pore volumes and average pore diameters of the catalysts were measured by N_2 adsorption–desorption isotherms at −196 °C using a Micromeritics ASAP 2020 M + C adsorption apparatus. The samples were degassed under vacuum at 200 °C for 6 h prior to measurement.

Temperature-programmed desorption of adsorbed CO (CO-TPD) was carried out in a quartz micro-reactor. The catalyst (0.1 g) was firstly reduced for 1.5 h at 350 °C in H_2 (10 mL/min), and then cooled down to 50 °C in He flow. The next step was CO adsorption at 50 °C for 30 min until the surface was saturated. Then the catalyst was swept with He for 1 h. Subsequently, the sample was heated in a flowing He stream (50 mL/min) up to 600 °C at a rate of 10 °C/min. The desorbed species were detected with a quadrupole mass spectrometer (QMS, Balzers Omnistar 200). MS signals at m/z = 28 (CO) and 44 (CO_2) were continuously recorded.

The structure of the supports and CO adsorption of the catalysts were studied using a Nicolet 6700 IR spectrometer equipped with a DRIFT (diffuse reflectance infrared Fourier transform) cell with CaF_2 windows. The sample in the cell was pretreated in H_2/N_2 (50 mL/min, V_{H2}/V_{N2} = 1:9) at 350 °C for 1 h, followed by N_2 (50 mL/min, Ultrahigh-purity) flushing at 350 °C for 0.5 h. After the temperature was dropped to 30 °C, the background was scanned in N_2. Followed by introducing 0.5% CO/N_2 (50 mL/min) into the IR cell, the IR spectrum of CO adsorbed on the catalyst was recorded at 30 °C, when adsorption state remained steady. The spectral resolution was 4 cm^{-1} and the number of scans was 64.

H_2 temperature-programmed reduction (H_2-TPR) was carried out in a quartz micro-reactor. Firstly, 0.05 g of the prepared catalyst was pretreated at 100 °C in N_2 for 1 h prior to a TPR measurement. During the TPR experiment, H_2/N_2 mixture gas with V_{H2}/V_{N2} = 1:9 was used at 50 mL/min and the temperature was ramped from 50 to 500 °C at a rate of 10 °C/min while the effluent gas was analyzed with a TCD.

The active copper surface areas (S_{Cu}) in the reduced catalysts were determined by the technique of N_2O reactive frontal chromatography at 60 °C assuming a Cu:N_2O = 2 titration stoichiometry and a surface atomic density of 1.46×10^{19} copper atoms m^{-2}, respectively.

Results and discussion

Characterization of SiO_2 supports

The IR spectra of the structure of the SiO_2 supports are presented in Fig. 1. It can be seen that a small absorption band at 970 cm^{-1} is observed on the support of SiO_2–H, which is ascribed to the symmetric stretching vibration of –OH group. Those at 804 cm^{-1} and 1100 cm^{-1} correspond to symmetric and asymmetric Si–O–Si stretching vibration, respectively. The absorption band at 1633 cm^{-1} is assigned to representative of absorbed water

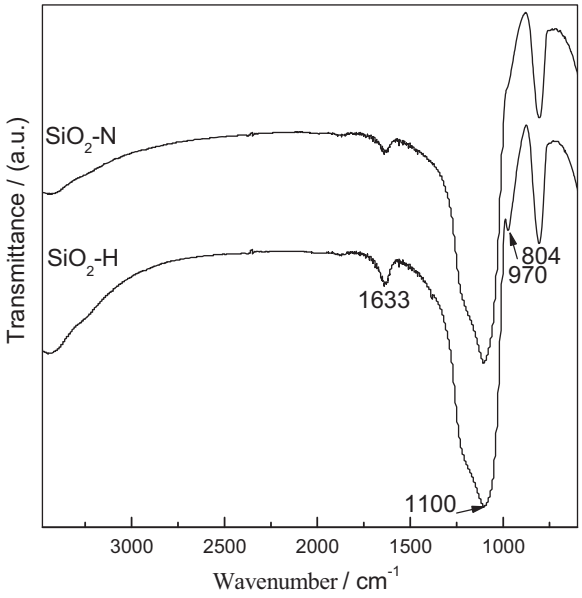

Fig. 1. FTIR spectra of the different SiO_2 supports.

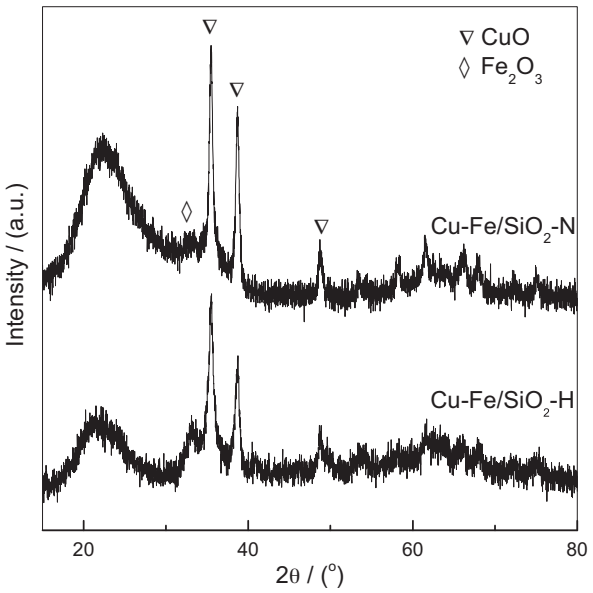

Fig. 2. XRD profiles of the different catalysts.

(H–O–H bending vibration) [29]. From Fig. 1, it can be noted that the Si–OH absorption band at 970 cm^{-1} disappeared on the support SiO_2–N, indicating that the concentration of Si–OH on the surface of support decreased significantly after the pretreatment with ammonia. The decrease in Si–OH concentration on the SiO_2 surface would suppress the interaction of active metals and support, which was favorable for increasing the dispersion of metals on the catalyst surface [20].

The BET surface areas, pore volumes, and average pore diameters of the supports are listed in Table 1. When the support SiO_2 was pretreated with ammonia, its specific surface area decreased sharply from 239.9 $m^2\,g^{-1}$ to 82.4 $m^2\,g^{-1}$, while the average pore diameter and pore volume increased from 5.7 nm and 0.69 $cm^3\,g^{-1}$ to 18.7 nm and 0.74 $cm^3\,g^{-1}$, respectively. The phenomenon was perhaps caused by the silica dissolving and skeleton collapsing when the support was pretreated with ammonia.

Characterization of the Cu–Fe/SiO_2 catalysts

N_2 adsorption and S_{Cu} measurement

The BET surface areas, pore volumes, and average pore diameters of the catalysts are also listed in Table 1. Similar to the supports, the catalyst Cu–Fe/SiO_2–N showed smaller surface area and larger pore diameter than those of the catalyst Cu–Fe/SiO_2–H. Moreover, dipping Cu/Fe on the support SiO_2–H led to a decrease in the surface area (from 239.9 $m^2\,g^{-1}$ to 208.0 $m^2\,g^{-1}$) and pore volume (from 0.69 $cm^3\,g^{-1}$ to 0.60 $cm^3\,g^{-1}$), which might occur from metals entered into and plugged some pores during the process of impregnation [30]. However, the specific surface area of Cu–Fe/SiO_2–N catalyst increased from 82.4 $m^2\,g^{-1}$ to 100.2 $m^2\,g^{-1}$ after Cu/Fe loaded on the support. It was probably caused by the copper oxide species with relatively small size (17.3 nm) deposited inside the larger mesopores (18.7 nm) of the support SiO_2–N, which also led to a remarkable decrease in the mean pore diameter of the catalyst Cu–Fe/SiO_2–N (11.2 nm) compared with support SiO_2–N (18.7 nm) [14].

In addition, as shown in Table 1, the active copper surface areas (S_{Cu}) of the catalyst Cu–Fe/SiO_2–N (3.06 $m^2\,g^{-1}$) was two times larger than that of the Cu–Fe/SiO_2–H catalyst (1.24 $m^2\,g^{-1}$). This was contrary to our initial expectation that the Cu–Fe/SiO_2–N catalyst would possess smaller S_{Cu} due to its small S_{BET}. This can be explained as follows: although the surface of SiO_2–N decreased when the support was pretreated by ammonia, the pore size of SiO_2–N increased by contrary. The CuO particles entered into and deposited inside the pores of Cu–Fe/SiO_2–N catalyst, forming the small pore structures on the inner walls of large pores, which made the outer surface of CuO particles in the large pores expose to reducing gas and be reduced more easily. The phenomenon resulted in the increased amount of active copper species [14]. And the increase in the amount of active copper species over the Cu–Fe/SiO_2–N will be favorable for improving the activity for the higher alcohols synthesis [31].

XRD results

Fig. 2 shows the XRD profiles of different catalysts after calcination at 350 °C for 4 h. As seen, the peak at 2θ of 33.3° corresponds to characteristic diffraction peak of α-Fe_2O_3 [32]

Table 1
Physicochemical properties of the samples.

Sample	S_{BET} [a]/($m^2\,g^{-1}$)	V_p [b]/($cm^3\,g^{-1}$)	D_p/nm	S_{Cu} [c]/($m^2\,g^{-1}$)	D_{CuO} [d]/nm
SiO_2–H	239.9	0.69	5.7	–	–
SiO_2–N	82.4	0.74	18.7	–	–
Cu–Fe/SiO_2–H	208.0	0.60	5.5	1.24	16.3
Cu–Fe/SiO_2–N	100.2	0.55	11.2	3.06	17.3

[a] The error of S_{BET} is ±1%.
[b] The error of V_p is ±2%.
[c] Determined by the technique of N_2O reactive frontal chromatography.
[d] Calculated from the Cu(1 1 1) peak of the XRD spectra according to the Scherrer equation, using the full width at half maxima values.

while those at 2θ of 35.6°, 38.7° and 48.8° could be ascribed to characteristic diffraction peaks of crystal CuO. The mean crystallite sizes of CuO calculated from the full width at half maximum of diffraction peak at $2\theta = 38.7°$ by Scherrer equation are listed in Table 1. It was found that the CuO particle size in both catalysts had no evident difference (16.3 nm vs. 17.3 nm). In addition, the diffraction peak of Fe_2O_3 was noticeably weakened on Cu–Fe/SiO_2–N compared with that on Cu–Fe/SiO_2–H, suggesting that Fe_2O_3 was finely dispersed on the surface of Cu–Fe/SiO_2–N catalyst.

Metal ions at silica–water interfaces would form complexes with the deprotonated surface silanol groups, and the interaction between metal and silica was strengthened with the concentration of Si–OH increasing, which could promote the dispersion of metal and result in the smaller metallic oxide particles [33,34]. Based on the view, the support pretreated by ammonia with lower concentration of Si–OH would lead to the larger metal oxide particles. However, according to the dynamic wettability of impregnation [35], at the later stage of evaporation of water, droplets of the impregnating solution could be formed on the surface of the support. More droplets formed on the hydrophobic surfaces than on the hydrophilic surfaces, which would easily cause the droplets to split or shrunk, resulting in the formation of smaller droplets than those on less hydrophobic surfaces. Each of these droplets would then produce some crystallites of metal precursors. As a result, the metal precursors may become more highly dispersed on more hydrophobic silica and form the smaller metal particles. So the particles of metal oxides would be smaller when the concentration of Si–OH on the surface of the support decreased.

Based on the above, when the support silica was pretreated by ammonia, although the decreased concentration of Si–OH weakened the interaction between metals and silica, the size of metal particles on Cu–Fe/SiO_2–N did not change obviously due to the formation of smaller droplets on more hydrophobic surfaces of SiO_2–N.

Temperature programmed reduction

Fig. 3 displays the H_2-TPR profiles of the catalysts. For the Cu–Fe/SiO_2–H catalyst, two peaks could be observed at about 230 °C and 256 °C, corresponding to the reduction of highly dispersed and bulk CuO, respectively [15]. Moreover, the broad peak detected at 400–500 °C was attributed to the reduction of Fe_2O_3 ($Fe_2O_3 \rightarrow Fe_3O_4 \rightarrow FeO \rightarrow Fe$) [36]. There was no obvious change for the reduction peak of iron species on the Cu–Fe/SiO_2–N, but the reduction peaks of CuO shifted slightly toward lower temperatures in comparison with those of Cu–Fe/SiO_2–H catalyst. It could be considered that the decrease in the density of Si–OH on surface of SiO_2 pretreated by ammonia weakened the interaction of metals-support, making the reduction of CuO more easy [14,37]. On the other hand, however, the decreased Si–OH may also enhance the interaction between copper and iron [32], which suppressed the reduction of CuO [15]. Thus, the reduction peaks of CuO shifted slightly toward low temperatures under the combined effects mentioned above.

Infrared spectra of CO adsorption

IR spectra of CO adsorption on different catalysts are shown in Fig. 4. Obviously, one peak at 2125 cm^{-1} was observed on Cu–Fe/SiO_2–H, corresponding to CO linearly adsorbed on copper species [38]. For the catalyst Cu–Fe/SiO_2–N, the intensity of the band enhanced substantially and the position shifted to a low wavenumber at 2109 cm^{-1} compared with that on Cu–Fe/SiO_2–H. The enhancement in the intensity of the band indicated that the CO adsorption ability of the copper was greatly strengthened over the Cu–Fe/SiO_2–N catalyst. This result is consistent with a higher S_{Cu} of the Cu–Fe/SiO_2–N catalyst obtained by N_2O determination, and suggests that the number of active sites increases on Cu–Fe/SiO_2–N catalyst. On the other hand, the shift of the absorption band to a low frequency can be ascribed to the strengthened Cu–CO bond [39,40]. Therefore, the ammonia modification of SiO_2 not only increased the amount of the active copper species on the catalyst surface but also strengthened the interaction of copper and iron, which resulted in the strengthened Cu–CO bond.

Temperature-programmed desorption of CO

The profiles of CO_2 desorption after CO adsorption on various catalysts are shown in Fig. 5. Two peaks of CO_2 desorption at about 140 °C and 450 °C were found on Cu–Fe/SiO_2–H, which indicated that there were two active centers for CO dissociation adsorption. It perhaps took place the CO dissociation or the disproportionation

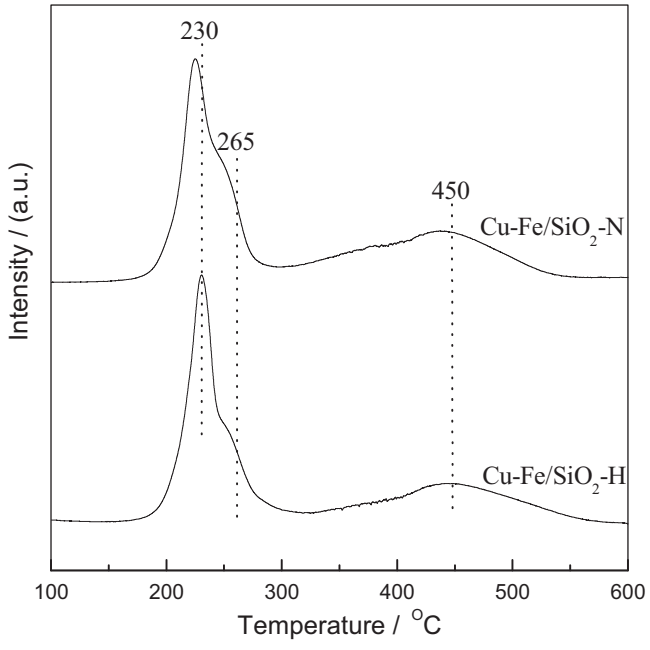

Fig. 3. H_2-TPR curves of the different Cu–Fe/SiO_2 catalysts.

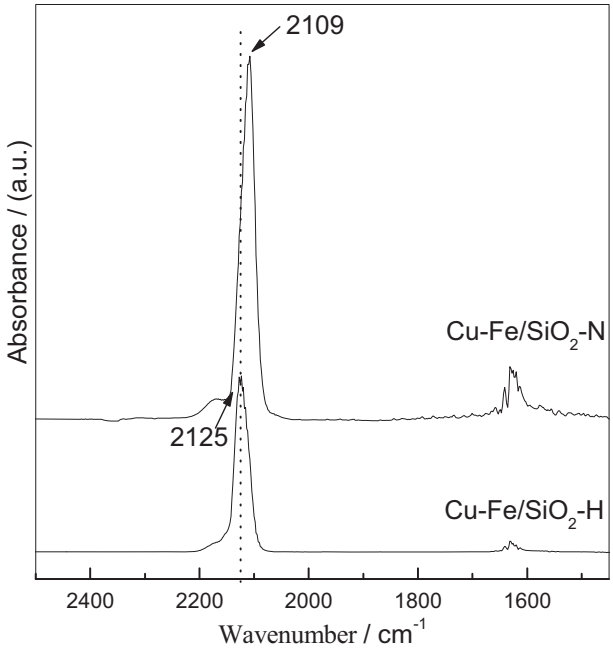

Fig. 4. IR spectra of CO chemisorbed on different catalysts.

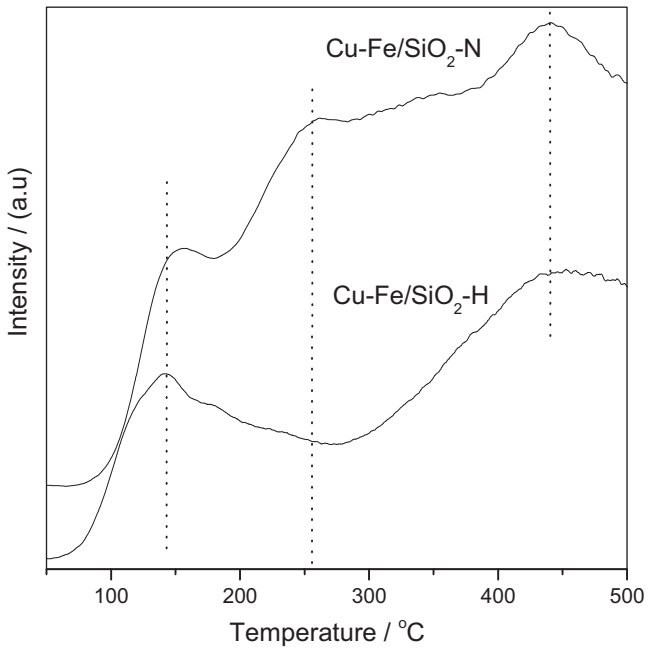

Fig. 5. CO_2-TPD spectra of different Cu–Fe/SiO_2 catalysts after adsorption of CO.

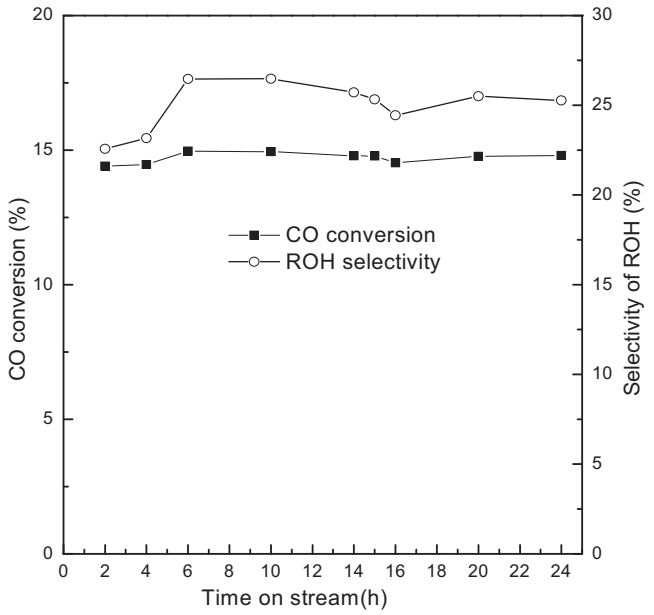

Fig. 6. CO conversion and alcohol selectivity vs. time-on-stream for the Cu–Fe/SiO_2–H catalyst. Reaction conditions: 250 °C, 3.0 MPa, $V(H_2)/V(CO) = 2$, $SV = 6000$ mL/(g h).

reaction ($2CO \rightarrow C + CO_2$) on the catalyst surface [41]. For the catalyst Cu–Fe/SiO_2–N, at the reaction temperature of CO hydrogenation (250 °C), there was a wide peak of CO_2 desorption. It suggests that when the temperature was at 250 °C, the dissociative capacity of CO adsorbed on the Cu–Fe/SiO_2–N catalyst was remarkably enhanced. Moreover, when the support was pretreated by ammonia, the peak of CO_2 desorption shifted to a higher temperature and the peak area increased, indicating that the intensity of CO adsorption strengthened and the number of active sites increased, which was in well agreement with the result of CO–IR characterization described above.

CO hydrogenation performances of the catalysts

Typical time dependent changes of CO conversion and alcohols selectivity over the representative Cu–Fe/SiO_2–H catalyst are shown in Fig. 6. It can be seen that both the CO conversion and alcohols selectivity increased during the first 6 h on stream, and remained relatively constant after 6 h on stream. Therefore, the data taken at 20–24 h on stream were used as indexes for reactivity of the catalysts and presented in Table 2.

As shown in Table 2, the catalyst Cu–Fe/SiO_2–H showed a normal catalytic performance, as indicated by the conversion of CO and the space time yield (STY) of ROH at 14.8% and 89.0 g kg^{-1} h^{-1}, respectively. However, the catalyst prepared from the ammonia-pretreated silica exhibited higher CO conversion and STY_{ROH}: the conversion of CO increased from 14.8% to 17.4%, and the STY_{ROH} increased from 89.0 g kg^{-1} h^{-1} to 107.0 g kg^{-1} h^{-1}.

According to the mechanism of CO hydrogenation to alcohols [6,7], the CO adsorbed on the catalyst either hydrogenates to methanol directly or dissociates to C^* and O^*, and then C^* hydrogenates to intermediate CH_x. On one hand, the CH_x hydrogenates to CH_4. On the other hand, CO inserts into metal-alkyl to form CH_xCO as the precursor of alcohols, which undergoes a further hydrogenation to ethanol. If the intermediate CH_x inserts into metal-alkyl, it will produce higher hydrocarbons. In addition, for the Cu–Fe-based catalysts, active copper species mainly serve as the sites for dissociative chemisorptions of hydrogen and the associative adsorption of CO, while active iron species act as sites for CO dissociation, C–C chain growth and hydrogenation [10]. Molecularly adsorbed CO on Cu migrates to the surface of Fe species followed by CO insertion into the metal-alkyl, and hydrogenation of CH_xCO groups produces alcohols. Therefore, the Cu–Fe synergistic effect plays an important role in the high activity of higher alcohol synthesis [11].

In the present work, for the catalyst Cu–Fe/SiO_2–N, the modification of support with ammonia increased the number of active copper species, which contributed to CO adsorption as evidenced by the result of FT-IR analysis, resulting in the increase of CO conversion. Moreover, when the support was pretreated by ammonia, the silica dissolved and resulted in the skeleton collapsing and the concentration of Si-OH decreasing. The former decreased the surface area sharply as shown in Table 1, and the latter enhanced the interaction between copper and iron, which was favorable for CO adsorption and dissociation. Combining the above results with the catalytic performance, it is inferred that the catalytic activity of Cu–Fe/SiO_2 was not determined by the surface area of the catalyst, and that the enhanced catalytic activity of Cu–Fe/SiO_2–N was mainly induced by more active copper species and the strengthened interaction between copper and iron [14].

Table 2
Performance of Cu-Fe/SiO_2 catalysts for CO hydrogenation reaction.

Catalyst	CO conv./%	Product selectivity/%				STY of ROH/g (kg h)$^{-1}$	Alcohol distribution/%	
		CO_2	CH_4	C_{2+}(HC)	ROH		CH_3OH	$C_{2+}OH$
Cu–Fe/SiO_2–H	14.8	13.0	7.4	51.8	27.8	89.0	70.9	29.1
Cu–Fe/SiO_2–N	17.4	13.1	7.4	50.9	28.6	107.0	69.9	30.1

Reaction conditions: 250 °C, 3.0 MPa, $V(H_2)/V(CO) = 2$, $SV = 6000$ mL/(g h).

Conclusions

The CO hydrogenation performance of Cu–Fe/SiO_2 catalyst was significantly improved by pretreating the silica support with ammonia: the CO conversion and the STY of ROH being increased from 14.8% and 89.0 g kg^{-1} h^{-1} to 17.4% and 107.0 g kg^{-1} h^{-1}, respectively. The improvements in the catalytic properties of the Cu–Fe/SiO_2–N catalyst were attributed to the decrease of Si–OH on support surface and increase of pore size, which enhanced the interaction between copper and iron and increased the amount of active sites of Cu. The synergistic effect between copper and iron can promote the dissociation of adsorbed CO, which was favorable for production of the intermediate CH_x. And more amounts of active sites of Cu can increase the capacity for CO adsorption. Both of them were responsible for the improved conversion of CO and ultimately increased the production of higher alcohols.

Acknowledgment

The authors acknowledge financial supports from the Science and Technology Commission of Shanghai Municipality (13ZR1461900, 08520513600).

References

[1] R.S. Venkateswara, K.D. Ajay, K. Janusz, Appl. Catal. A: Gen. 404 (2011) 1–11.
[2] V. Subramani, S.K. Gangwal, Energy Fuels 22 (2008) 814–839.
[3] J. Yu, D.S. Mao, L.P. Han, Q.S. Guo, G.Z. Lu, J. Ind. Eng. Chem. 19 (2013) 806–812.
[4] M. Gupta, J.J. Spivey, Catal. Today 147 (2009) 126–132.
[5] X.H. Mo, Y.T. Tsai, J. Gao, D.S. Mao, J.G. Goodwin Jr., J. Catal. 285 (2012) 208–215.
[6] K. Xiao, Z.H. Bao, X.Z. Qi, X.X. Wang, L.S. Zhong, K.G. Fang, M.G. Lin, Y.H. Sun, Chin. J. Catal. 34 (2013) 116–129.
[7] K.G. Fang, D.B. Li, M.G. Lin, M.L. Xiang, W. Wei, Y.H. Sun, Catal. Today 147 (2009) 133–138.
[8] M. Gupta, M.L. Smith, J.J. Spivey, ACS Catal. 1 (2011) 641–656.
[9] M.G. Lin, K.G. Fang, D.B. Li, Y.H. Sun, Catal. Commun. 9 (2008) 1869–1873.
[10] Y.W. Lu, F. Yu, J. Hu, J. Liu, Appl. Catal. A: Gen. 429–430 (2012) 48–58.
[11] W. Gao, Y.F. Zhao, J.M. Liu, Q.W. Huang, S. He, C.M. Li, J.W. Zhao, M. Wei, Catal. Sci. Technol. 3 (2013) 1324–1332.
[12] M.Y. Ding, J.G. Liu, Q. Zhang, N. Tsubaki, T.J. Wang, L.L. Ma, Catal. Commun. 28 (2012) 138–142.
[13] K. Xiao, X.Z. Qi, Z.H. Bao, X.X. Wang, L.S. Zhong, K.G. Fang, M.G. Lin, Y.H. Sun, Catal. Sci. Technol. 3 (2013) 1591–1602.
[14] S. Kiatphuengporn, M. Chareonpanich, J. Limtrakul, Chem. Eng. J. 240 (2014) 527–533.
[15] H. Zhang, W. Chu, H.Y. Xu, J. Zhou, Fuel 89 (2010) 3127–3131.
[16] X.M. Yang, Y. Wei, Y.L. Su, L.P. Zhou, Fuel Process. Technol. 91 (2010) 1168–1173.
[17] S.K. Das, S. Majhi, P. Mohanty, K.K. Pant, Fuel Process. Technol. 118 (2014) 82–89.
[18] M.Y. Ding, M.H. Qiu, J.G. Liu, Y.P. Li, T.J. Wang, L.L. Ma, Fuel 109 (2013) 21–27.
[19] Q.S. Guo, D.S. Mao, J. Yu, L.P. Han, J. Fuel Chem. Technol. 40 (2012) 1103–1107.
[20] D.H. Jiang, Y.J. Ding, Z.D. Pan, W.M. Chen, H.Y. Luo, Catal. Lett. 121 (2008) 241–246.
[21] L.P. Han, D.S. Mao, J. Yu, Q.S. Guo, G.Z. Lu, Catal. Commun. 23 (2012) 20–24.
[22] J. Yu, D.S. Mao, L.P. Han, Q.S. Guo, G.Z. Lu, Fuel Process. Technol. 106 (2013) 344–349.
[23] L.P. Han, D.S. Mao, J. Yu, Q.S. Guo, G.Z. Lu, Appl. Catal. A: Gen. 454 (2013) 81–87.
[24] Y. Zhang, K. Hanayama, N. Tsubaki, Catal. Commun. 7 (2006) 251–254.
[25] R.Y. Xie, D.B. Li, B. Hou, J.G. Wang, L.T. Jia, Y.H. Sun, Catal. Commun. 12 (2011) 589–592.
[26] X.Y. Lv, J.F. Chen, Y.S. Tan, Y. Zhang, Catal. Commun. 20 (2012) 6–11.
[27] L.H. Shi, D.B. Li, B. Hou, Y.L. Wang, Y.H. Sun, Fuel Process. Technol. 91 (2010) 394–398.
[28] J.L. Zhang, J.G. Chen, J. Ren, Y.H. Sun, Appl. Catal. A: Gen. 243 (2003) 121–131.
[29] P.R. Pinto, L.C. Mendes, M.L. Dias, C. Azuma, Colloid Polym. Sci. 284 (2006) 529–535.
[30] H. Zheng, D. Hu, L. Zhang, C. Ma, T. Rufford, Miner. Eng. 35 (2012) 20–26.
[31] V. Mahdavi, M.H. Peyrovi, M. Islami, J.Y. Mehr, Appl. Catal. A: Gen. 281 (2005) 259–265.
[32] J.G. Liu, M.Y. Ding, T.J. Wang, L.L. Ma, Acta Phys. Chim. Sin. 28 (2012) 1964–1970.
[33] P.W. Schindler, B. Füret, R. Dick, P.U. Wolf, J. Colloid Interf. Sci. 55 (1976) 469–475.
[34] L.H. Shi, D.B. Li, B. Hou, Y.H. Sun, Chin. J. Catal. 28 (2007) 999–1002.
[35] S.L. Guo, M. Arai, Y. Nishiyama, Appl. Catal. 65 (1990) 31–44.
[36] C.H. Zhang, Y. Yang, B.T. Teng, T.Z. Li, H.Y. Zheng, H.W. Xiang, Y.W. Li, J. Catal. 237 (2006) 405–415.
[37] M.Y. Ding, J.L. Tu, J.G. Liu, N. Tsubaki, T.J. Wang, L.L. Ma, Catal. Today 234 (2014) 278–284.
[38] R. Xu, Z.Y. Ma, C. Yang, W. Wei, W.H. Li, Y.H. Sun, J. Mol. Catal. A: Chem. 218 (2004) 133–140.
[39] R. Xu, Z.Y. Ma, C. Yang, W. Wei, Y.H. Sun, React. Kinet. Catal. Lett. 81 (2004) 91–98.
[40] G. Blyholder, M. Lawless, Surf. Sci. 290 (1993) 155–162.
[41] C. Mazzocchia, P. Gronchi, A. Kaddouri, E. Tempesti, L. Zanderighi, A. Kiennemann, J. Mol. Catal. A: Chem. 165 (2001) 219–230.